Ripple-Free High-Power Super-Luminescent Diode Arrays

F. Causa, *Member, IEEE*, and L. Burrow

***Abstract*—This paper presents the experimental and theoretical characterisation of arrays of tapered super-luminescent diodes to achieve very high, broad-band, ripple-free optical output. These arrays were fabricated from 980-nm high-power triple-quantum-well InGaAs–AlGaAs double heterostructures. Output powers of 2.7 W pulsed and of 280-mW quasi-CW were obtained from antireflection-coated arrays, with 10% maximum wall-plug efficiency per pulse at 0.75-W pulsed output power. Experimental and theoretical results for the optical-electrical characteristics and the near- and far-field radiation characteristics of the arrays are discussed and compared with those of corresponding individual super-luminescent diodes.**

***Index Terms*—Arrays, high-power, near and far fields, ripple-free spectrum, super-luminescent diodes.**

I. Introduction

SUPER-LUMINESCENT diodes (SLDs) are broadband, typically high-power, semiconductor optical sources used for applications including optical coherence tomography [1], wavelength division multiplexing [2], fiber-optic gyroscopes [3], short-haul communications, military applications, and illumination [4]. The key device feature necessary to achieve super-luminescent operation with low spectral modulation is low effective facet reflectivity to eliminate optical feedback (Fabry–Pérot resonances) and, therefore, avoid lasing. Several techniques have been proposed in the literature to achieve low effective reflectivity, including antireflection (AR) coating of the device facets (obtaining essentially a laser operated below threshold), unpumped absorption region at the rear of the device [5], bent [6] or angled [7] current injection contact, and etched deflector to deflect the unwanted reverse-traveling optical signal into the substrate [8]. By using the latter technique, output powers in excess of 1.3 W (at 3 kA $\cdot$ cm^{-2} pulsed injection current density) were obtained from in-house designed and fabricated AR-coated SLDs with tapered-geometry injection contact to reduce optical gain saturation [9]. To further increase the output power while maintaining the desired spectral and radiation properties and without compromising on the wall-plug efficiency achieved with conventional SLDs, a novel array of tapered SLDs (TSLDs) was designed and fabricated in-house. This paper presents the design and characterization of such TSLD arrays (TSLDAs) with which output optical powers in excess of 2.7 W were achieved at 3 kA $\cdot$ cm^{-2} pulsed, with ripple-free output spectrum. To provide useful comparisons, several TSLDAs were fabricated and characterized in house with different numbers of elements, referred to as N-TSLDAs, with $N = 3, 4, 5$. This paper is organized as follows. The device structure and characteristics are described in Section II, and the experimental and corresponding results obtained from in-house developed models are presented and discussed in Section III, with the most relevant conclusions summarized in Section IV.

TABLE I
EPITAXIAL LAYERS OF HIGH-POWER, LARGE-OPTICAL-CAVITY, TRIPLE-QW InGaAs–GaAs–AlGaAs MATERIAL USED FOR DEVICE FABRICATION

Layer	Thickness	Composition	Doping	Dopant
Capping	0.18 μm	GaAs	3.9×10^{19} cm^{-3}	Zn
Cladding	0.75 μm	$Al_{0.41}Ga_{0.59}As$	2×10^{18} cm^{-3}	C
Guide	0.33 μm	$Al_{0.2}Ga_{0.8}As$	undoped	-
Barrier	10 nm	GaAs	undoped	-
QW	7 nm	$In_{0.17}Ga_{0.83}As$	undoped	-
Barrier	10 nm	GaAs	undoped	-
QW	7 nm	$In_{0.17}Ga_{0.83}As$	undoped	-
Barrier	10 nm	GaAs	undoped	-
QW	7 nm	$In_{0.17}Ga_{0.83}As$	undoped	-
Barrier	10 nm	GaAs	undoped	-
Guide	0.33 μm	$Al_{0.2}Ga_{0.8}As$	undoped	Si
Cladding	0.76 μm	$Al_{0.41}Ga_{0.59}As$	9×10^{17} cm^{-3}	Si
Buffer	0.5 μm	GaAs	1×10^{18} cm^{-3}	Si

II. Device Structure

The TSLDAs were fabricated from a MOVPE-grown, high-power, large-optical-cavity, strained InGaAs–AlGaAs double-heterostructure material. The active layer is composed of three 7-nm InGaAs quantum wells (QWs) separated by 10-nm GaAs barriers (see Table I) for emission at 980 nm. The schematic of the TSLDA is presented in Fig. 1. To suppress lasing from each individual element in the array, a V-groove deflector was ion-beam etched at 45° with respect to the output facet. The distance of the deflector from the taper edge is $D = 200$ μm. To prevent optical propagation across devices and reduce optical gain saturation, additional V-groove deflectors were etched longitudinally to optically separate the elements in the array. Other relevant device dimensions are presented in Table II.

In correspondence to the tapered injection contacts delineating the elements in the array, shallow ridges (etch depth

Manuscript received March 6, 2007; revised June 26, 2007.

The authors are with the Department of Electronic and Electrical Engineering, University of Bath, Bath BA2 7AY, U.K. (e-mail: f.causa@bath.ac.uk; L.Burrow@bath.ac.uk).

Color versions of one or more of the figures in this paper are available online at http://ieeexplore.ieee.org.

Digital Object Identifier 10.1109/JQE.2007.905291

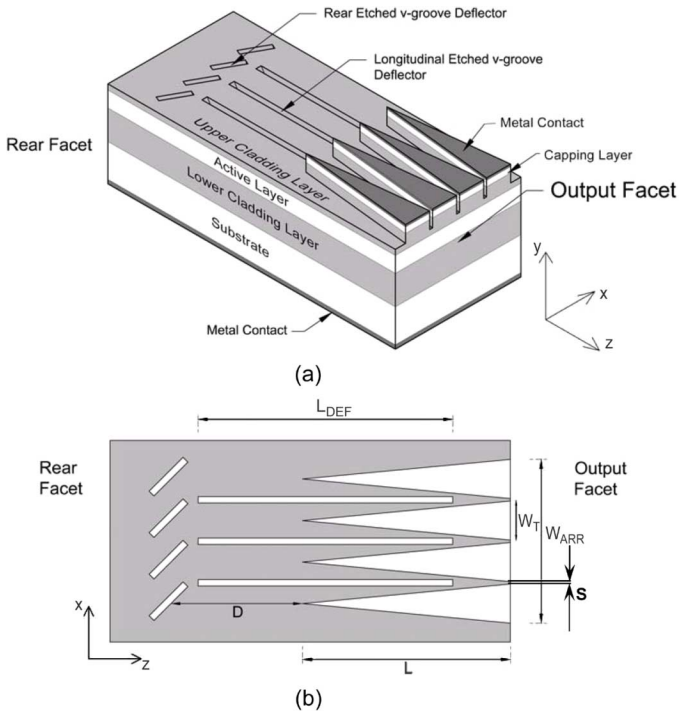

Fig. 1. (a) Schematic representation of four-element TSLDA. (b) Top-view schematic with main parameters.

TABLE II
TSLDA DEVICE DIMENSIONS

Parameter	Symbol	Value (μm)
Length	L	1000
Element width at output facet	W_T	100
Output facet width	W_{ARR}	$N \times W_T$
Length of longitudinal deflector	L_{DEF}	900
Distance between rear deflector and taper vertex	D	200

~ 0.3 μm) were ion-beam-etched through the capping layer (see Fig. 1) to efficiently reduce current spreading, but without providing lateral (effective) refractive index step. The TSLDAs were mounted n-side down onto a copper heat sink using a conductive silver-loaded epoxy resin. The p-side was contacted with gold wire using a thermo-compression ultrasonic bonder. The device output facet was AR-coated with a single layer of ZrO_2–TiO_2 reducing the reflectivity to approximately 1%. Several N-TSLDAs were fabricated in house with $N = 3, 4, 5$. The measured operational characteristics are presented in Section III and compared with those of individual TSLDs [9]. It is noted here that, because of the nonoptimal heat-sinking properties of the present device and mount configuration, all devices were measured under pulsed conditions (5 μs, 200 Hz).

III. DEVICE CHARACTERIZATION

The voltage-injection current (V–I) characteristics measured from N-TSLDA (with $N = 3, 4, 5$) elements are compared in Fig. 2 with those obtained from an individual TSLD ($N = 1$). The estimated series resistance R_S of the devices increases slightly with the number of elements in the array, as indicated

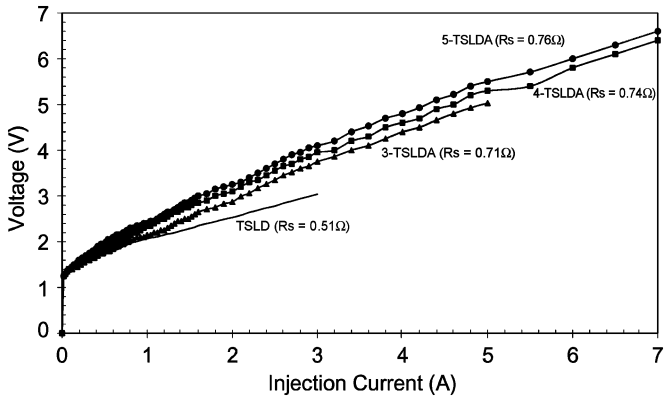

Fig. 2. Voltage–current characteristic measured from uncoated N-TSLDAs: $N = 1$ (solid line); $N = 3$ (solid line with triangles); $N = 4$ (solid line with squares); $N = 5$ (solid line with circles).

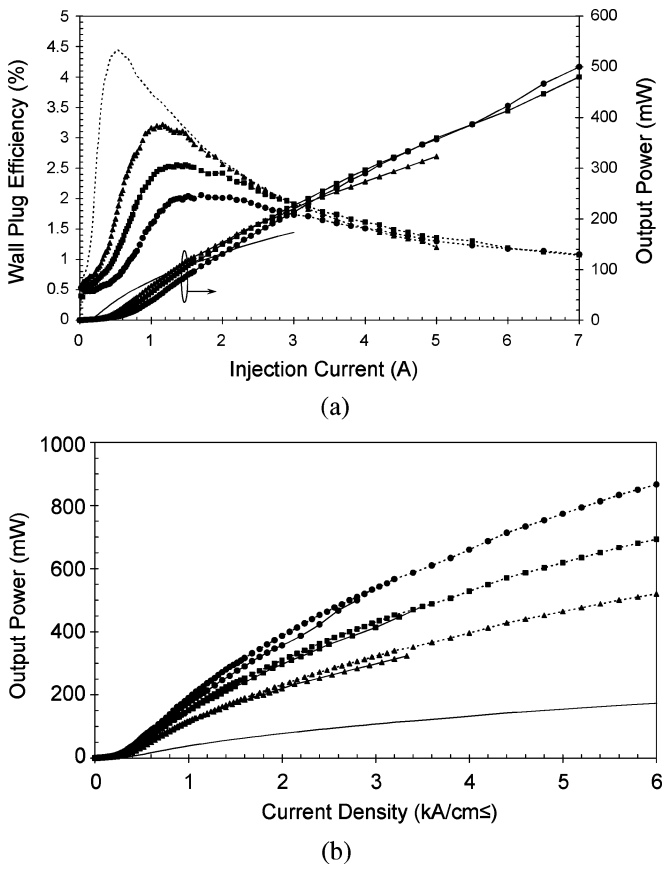

Fig. 3. (a) Experimental output optical power–current characteristics (solid line) measured from N-TSLDAs with $N = 1$ (solid curve), 3 (solid curve with triangles), 4 (solid curve with squares), 5 (solid curve with circles), and corresponding W-P efficiency (dashed curves with same symbols). (b) Experimental (solid line) and estimated (dashed line) output power as a function of current density for N-TSLDAs with $N = 1, 3, 4, 5$, as above (Pulse width $= 5$ μ s; repetition rate $= 200$ Hz).

in Fig. 2. The slight increase in R_S is attributed to the sheet resistance of the TiAu p-contact, which is proportional to the contact area [10].

The optical output power as a function of the injection current characteristics and wall-plug (W-P) efficiency measured from uncoated N-TSLDAs (with $N = 3, 4, 5$) are compared in Fig. 3(a) with corresponding ones measured from individual

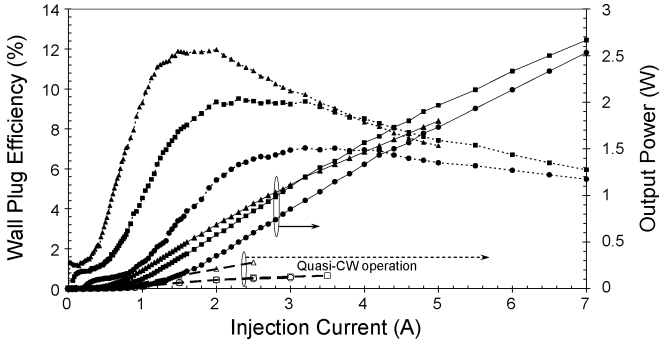

Fig. 4. Experimental pulsed (1 μs/1 ms) power–current characteristics (solid line) measured from AR-coated N-TSLDAs with $N = 3$ (triangles), 4 (squares), and 5 (circles) and corresponding W-P efficiency curves (dashed). Corresponding curves measured under quasi-CW operation $(1\ \mu\text{s}/10\ \mu\text{s})$ are also included (corresponding, open symbols, dashed curves).

TSLDs. These curves present the typical characteristics of super-luminescent operation, namely the three regions of linear regime when the optical gain is nonpositive (spontaneous emission), the super-linear regime at the onset of superluminescence when the optical gain is positive (amplified spontaneous emission), and the sublinear regime when optical gain saturation occurs. The maximum output power measured from uncoated 5-TSLDAs is 500 mW at $I = 7$ A (corresponding to $J = 2.8$ kA $\cdot$ cm^{-2} current density). Although the output power scales almost exactly with the number N of elements, the W-P efficiency of the arrays is significantly reduced with respect to that of an individual device $(N = 1)$ because the arrays require a larger operating voltage. The same data is presented in Fig. 3(b) in terms of injection current density to highlight the scaling of the output power as a function of the number of elements in the array. In the same plot of Fig. 3(b), corresponding theoretical curves are included for comparison. These were obtained by simply multiplying the output power calculated from an individual device by the number N of devices in the array. The output power measured from N-TSLDAs is the same as that expected from N separate TSLDs—this result confirms that the elements in the array are independent and that, therefore, the arrays are incoherent sources as desired.

After AR coating of the output facet to achieve a 1% output facet reflectivity, a substantial five-fold increase in output power is observed [9], with a corresponding increase in W-P efficiency (see Fig. 4). The highest output power was measured from AR-4-TSLDA to be 2.7 W at $I = 7$ A (equivalent to 3.5 kA $\cdot$ cm^{-2} current density) without breaking the devices. The maximum conversion (W-P) efficiency observed from such devices was 10% at 0.75-W pulsed output power. The 2.5-W output power measured from the AR-5-TSLDA is lower than expected because of the poor quality of the AR coating on that particular device.

The pulse rate was then reduced to a quasi-CW level of 1:10 $(1\ \mu\text{s}/10\ \mu\text{s})$ (see Fig. 4; corresponding open symbols, dashed lines), obtaining 280-mW output at 2.5 A from AR-3TSLDA and about 140 and 115 mW at 3.5 and 3 A from AR-4TSLDAs and AR-5TSLDAs, respectively.

CW measurements were also attempted, but, since devices are mounted p-side up, the thermal management is very poor. The devices could be measured under CW operation up to a current of 450 mA, obtaining 5-mW output power, which is approximately 20% of the power obtained under pulsed operation at correspondingly low injection current levels. To operate such devices under CW operation, it will be necessary to improve the thermal management. This can be achieved by mounting the devices p-side down, improving the metal contact and bonding and package the device on a thermally controlled heat sink.

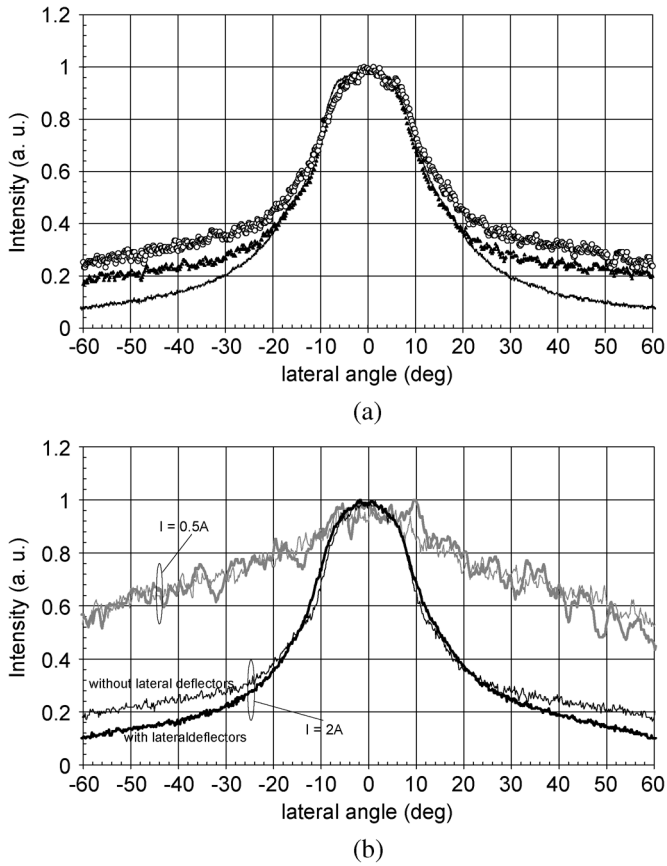

Fig. 5. (a) Lateral far-field intensity profiles measured from N-TSLDAs with $N = 1$ (solid line), 3 (triangles), 4 (squares), and 5 (circles) at $J = 3$ kA$\cdot$cm^{-2}. (b) Far-field intensity profiles measured from 4-TSLDAs with and without separation between individual taper elements at 0.5 and 2 A.

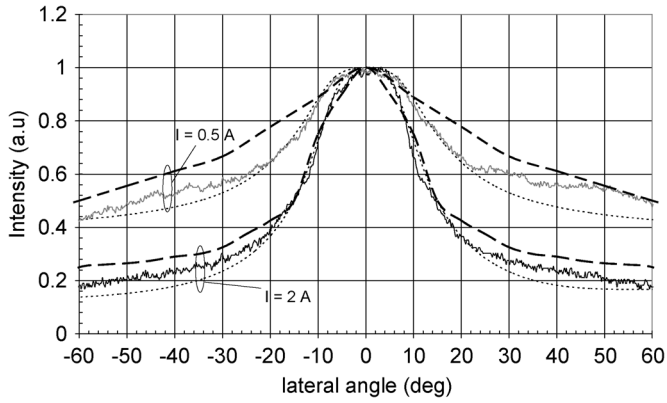

Fig. 6. Experimental lateral far-field intensity profiles measured from 4-TSLDAs under pulsed (solid line) and quasi-CW (dashed line) operation, at $I = 0.5$ A and $I = 2$ A and corresponding theoretical profiles (dotted line).

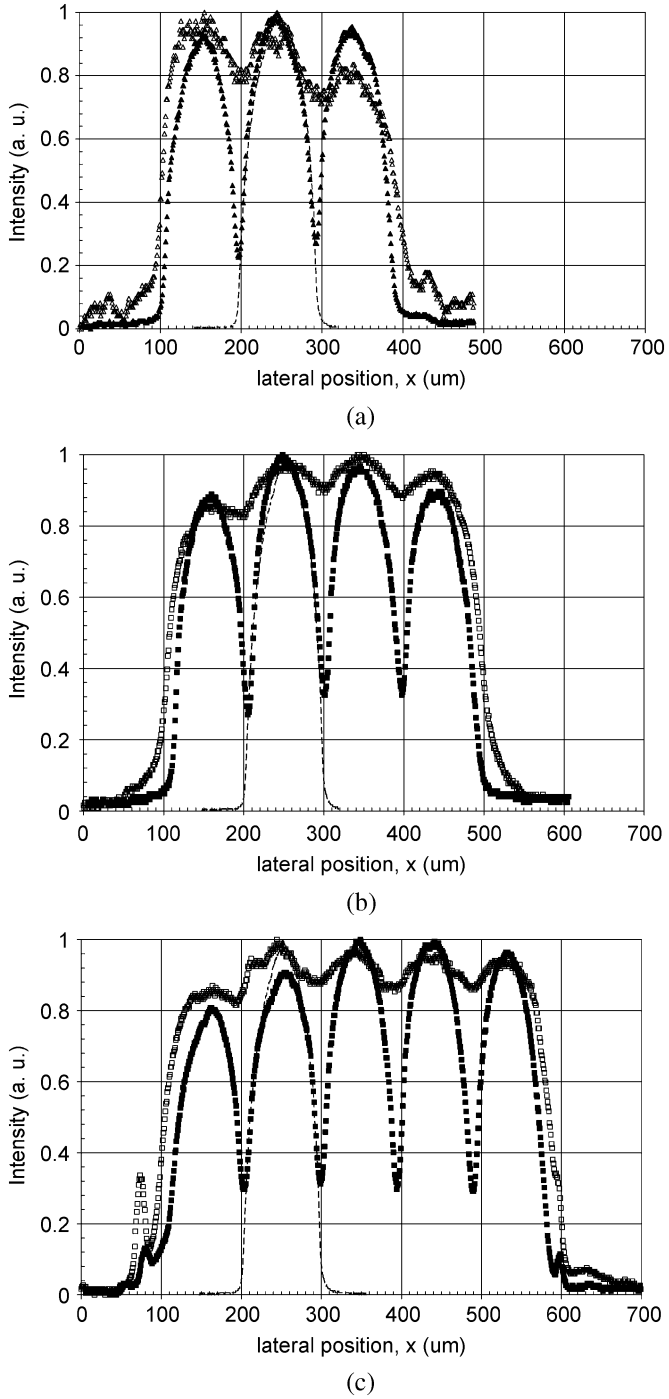

Fig. 7. Experimental near-field intensity profiles obtained at $J = 0.5$ and 3 kA $\cdot$ cm^{-2} current density from (a) 3-TSLDAs (open triangles: $I = 750$ mA; full triangles: $I = 4.5$ A), (b) 4-TSLDAs (open squares: I = 1 A; full squares: $I = 6$ A), (c) 5-TSLDAs (open circles: $I = 1.25$ A; full circles: $I = 7$ A). In all cases, the near-field profile obtained from an individual TSLD (dashed line) at $J = 3$ kA $\cdot$ cm^{-2} is included for comparison.

The far-field intensity profiles measured at $J = 3$ kA $\cdot$ cm^{-2} from arrays with $N = 3, 4$, and 5 elements are presented in Fig. 5(a) and compared with those typically measured from individual devices of corresponding geometry. As expected, the far-field characteristics of the arrays are not significantly different from those of individual TSLDs, confirming the efficacy of the longitudinal V-groove deflectors. The lateral far-field full-

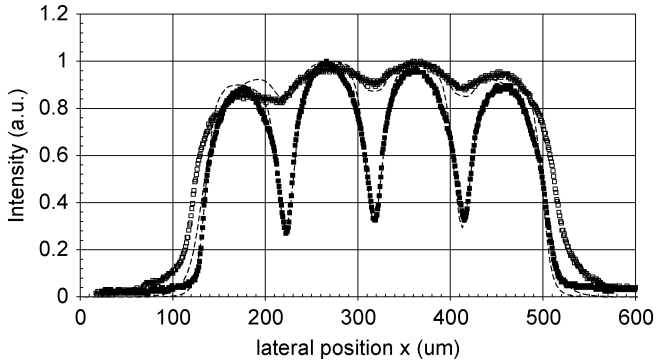

Fig. 8. Theoretical (dashed line) and experimental NF intensity profiles obtained for 4-T-SLDAs at $J = 0.5$ kA $\cdot$ cm^{-2} (open squares) and $J = 3$ kA $\cdot$ cm^{-2} (full squares).

width at half-maximum (FWHM) is approximately 30° for all devices. The only difference between the far-field profiles is that those measured from the arrays present more prominent shoulders. This appreciable background illumination is attributed to rays traveling at wide angles crossing the active and passive regions between the injection contacts of the elements in the arrays. To verify the above statement and, thus, eliminate such wide-angle radiation, arrays with individual elements with separate output facets were fabricated and characterized. A separation ($S = 10$ μm) of three to four times the carrier diffusion length ($L \sim 3$ μm) was considered to be sufficient to completely separate the elements. As demonstrated by the improved far-field profiles presented in Fig. 5(b), the wide-angle rays were efficiently attenuated by the unpumped regions between the elements in the arrays. All of the experimental curves obtained from the devices presented here are validated by theoretical far-field intensity profiles obtained from in-house-developed ray models [11]. As a representative example, the experimental and theoretical lateral far-field pattern obtained from 4-TSLDAs at different injection currents under pulsed and quasi-CW operation are plotted in Fig. 6, noting that the patterns are similar.

The characterization of the near field provides information on device quality and on the uniformity of the material and the injection profile. The experimental near-field intensity profiles detected from N-TSLDAs with $N = 3, 4$, and 5 at different current densities are presented in Fig. 7. From the uniformity and absence of interference effects in the measured profiles, it is possible to infer that, as expected, the individual elements in the arrays are operating independently. In addition, the peaks of the intensity profiles are at the same level for all arrays, indicating a uniform distribution of carriers across the array. The theoretical results obtained from the model [11] closely match the experimental profiles, as shown in Fig. 8, for the case $N = 4$.

Spectral measurements were taken using an optical spectrum analyzer (ANDO AQ6317B). Spectra measured from 4-TSLDAs and from individual TSLDs at $J = 3$ kA $\cdot$ cm^{-2} are compared in Fig. 9(a) (0.1-nm resolution). These results indicate that the arrays remain broadband, with essentially unmodulated spectrum. Thus, the characteristics of the arrays are similar to those of individual SLDs [9]: the FWHM spectral width is $\Delta\lambda = 18$ nm, corresponding to $L_c = 0.66(\lambda^2/\Delta\lambda) \cong 35$ μm coherence length, with <0.1-dB modulation. The modal

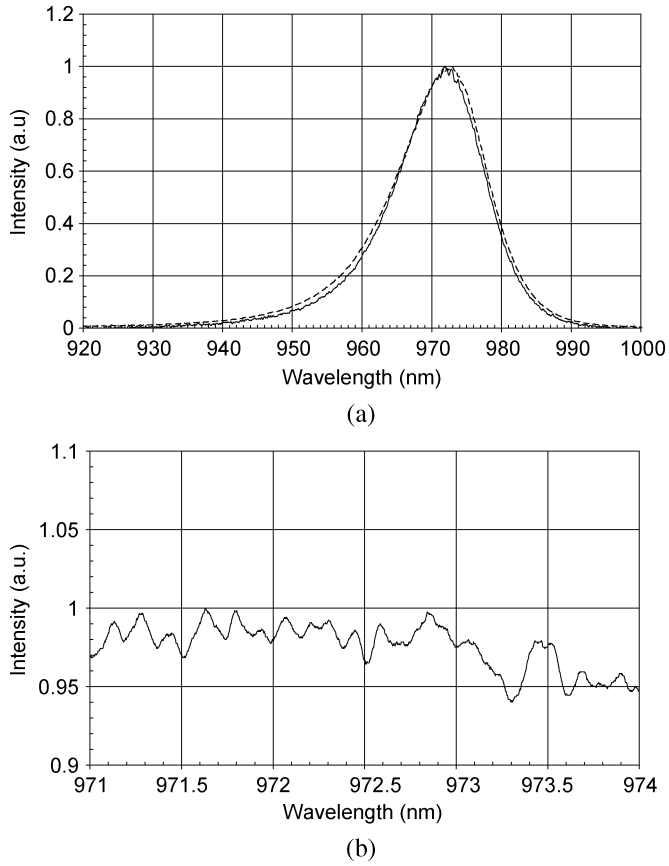

Fig. 9. (a) Output spectra measured from 4-TSLDAs (solid curve) and from an individual TSLD (dashed curve) at $J = 3$ kA $\cdot$ cm^{-2} (0.1-nm resolution). (b) Modulation of the peak of the spectrum measured from 4-TSLDA at the same current density (0.01-nm resolution).

spacing was estimated to be approximately 0.1 nm from the intensity ripple at the peak of the measured spectrum (0.01-nm resolution) [see Fig. 9(b)], which is in agreement with the theoretical estimate of 0.119 nm [9].

IV. Conclusion

The experimental and theoretical characterization of arrays of tapered super-luminescent diodes was presented. Output powers in excess of 2.7 W with 10% W-P efficiency were obtained from AR-coated arrays of tapered super-luminescent diodes. The output power measured from the arrays was found to be scaling almost exactly with the number of elements in the array. This observation confirms that the individual elements are working independently, as demonstrated also by the near and far radiation pattern characteristics of the devices. To achieve robust CW operation, it will be necessary to improve the packaging and thermal management of the devices. The output spectra measured from these high-power arrays are essentially ripple-free, with a negligible modulation of <0.1 dB.

References

[1] R. Tripathi, N. Nassif, J. S. Nelson, B. H. Park, and J. F. de Boer, "Spectral shaping for non-Gaussian source spectra in optical coherence tomography," *Opt. Lett.*, vol. 27, no. 6, pp. 406–407, March 15, 2002.

[2] B. Mikulla, L. Leng, S. Bears, B. C. Collings, M. Arend, and K. Bergman, "Broad-band high-repetition-rate source for spectrally sliced WDM," *IEEE Photon. Technol. Lett.*, vol. 11, no. 4, pp. 418–420, Apr. 1999.

[3] W. K. Burns, C. L. Chen, and R. P. Moeller, "Fiber-optic gyroscopes with broad-band sources," *J. Lightw. Technol.*, vol. LT-1, no. 1, pp. 98–105, Mar. 1983.

[4] S. Peralta and H. Ruda, "Applications for advanced solid-state lamps," *IEEE Ind. Applic. Mag.*, pp. 31–42, Jul./Aug. 1998.

[5] J. H. Song, S. H. Cho, I. K. Han, Y. Hu, P. J. S. Heim, F. G. Johnson, D. R. Stone, and M. Dagenais, "High-power broad-band Superluminescent Diode with low spectral modulation at 1.5 um wavelength," *IEEE Photon. Technol. Lett.*, vol. 12, no. 7, pp. 783–785, Jul. 2000.

[6] C.-F. Lin and C.-S. Juang, "Superluminescent diodes with bent waveguide," *IEEE Photon. Technol. Lett.*, vol. 8, no. 2, pp. 206–208, Feb. 1996.

[7] M. Sugo, Y. Shibata, H. Kamioka, M. Yamamoto, and Y. Tohmori, "High-power ($>$50 mW) and wideband ($>$50 nm) 1.3 μm superluminescent diodes," *Electron. Lett.*, vol. 41, no. 8, Apr. 2005.

[8] I. Middlemast, J. Sarma, and S. Yunus, "High power tapered superluminescent diodes using novel etched deflectors," *Electron. Lett.*, vol. 33, no. 10, pp. 903–904, May 1997.

[9] L. Burrow, F. Causa, and J. Sarma, "1.3 W ripple-free superluminescent diode," *IEEE Photon. Technol. Lett.*, vol. 17, no. 9, pp. 2035–2037, Sep. 2005.

[10] R. F. Reyna, A. Marti, C. Algora, J. C. Maroto, and G. L. Araujo, "Influence of size factors in the electroluminescent emission of large area GaAs IRED's," *IEEE Trans. Electron Devices*, vol. 44, no. 7, pp. 1174–1176, Jul. 1997.

[11] F. Causa and J. Sarma, "A realistic model for the output beam profile of stripe and tapered superluminescent LEDs," *Appl. Opt.*, vol. 42, no. 21, pp. 4341–4348, Jul. 2003.

F. Causa (M'98) received the Laurea degree in physics from the University of Milan, Milan, Italy, in 1993, and the Ph.D. degree from the University of Bath, Bath, U.K., in 1998.

She joined the Department of Electronic and Electrical Engineering, University of Bath, as a Lecturer in 1999. Her research experience includes the modeling, design, and characterization of semiconductor optical devices. In 2001, she was seconded to Bookham Technology, Caswell, U.K., to work on tapered geometry optical devices for a period of six months via an Industrial Secondment Scheme funded by the Royal Academy of Engineering. Recently, she collaborated with scientists at the Max Born Institute fur Nichtlineare Optik und Kurzzeitspectroscopie, Berlin, Germany (VI European Framework Programme Laser-Lab Europe for the characterization of advanced high brightness semiconductor sources, 2005), and Padova University (British-Italian partnership program for young researchers, sponsored by the British Council for the use of high-brightness parabolic laser arrays in medicine, 2006). Her present research interests include the development of high-brightness laser diodes and arrays, high-power super-luminescent diodes, and optical devices for sensing and modeling of nonlinear optical media.

L. Burrow received the M.Eng. and Ph.D. degrees from the Department of Electronic and Electrical Engineering, University of Bath, Bath, U.K., in 2001 and 2006, respectively.

His main research interest is in high-power super-luminescent diode design, fabrication, and characterization. He is currently on leave from the University of Bath.